DYNAMIC LANDING SITE RANKING FOR HELICOPTER EMERGENCY SITUATIONS

Michael Zimmermann*, Niklas Peinecke**
German Aerospace Center (DLR),
* Institute of Flight Systems, ** Institute of Flight Guidance
Lilienthalplatz 7, 38108 Braunschweig, Germany

ABSTRACT

Landing on unprepared sites is a typical mission task in day-to-day helicopter operations. Right after the event of an emergency which requires an immediate landing, the choice of a proper landing site is one of various time-critical and vital tasks which a helicopter pilot has to handle under intensive stress. This paper proposes a preventive procedure of landing site ranking to guide the pilot's attention to places with an increased chance of survivability. For that purpose, LIDAR data acquired during the flight by DLR's research rotorcraft ACT/FHS (Active Control Technology/Flying Helicopter Simulator, a highly modified EC135) is used for algorithm development and demonstration. Three types of results are shown. Starting with a landing site test-geometry, the algorithm's capabilities are demonstrated based on LIDAR data generated in DLR's AVES flight simulator. Secondly, a test-case using recorded LIDAR data acquired during previous flight tests is shown as an example close to real life with additional emergency ranking. Since wind is a major influence factor when choosing an appropriate landing site, varying ranking results of the real-life testcase with head-, cross- and rearwind conditions complete this paper.

Acronyms

ACT/FHS	Advanced Control Technology/ Flying Helicopter Simulator
AR	Autorotation
AVES	Air VEhicle Simulator
CoALa	Communication & Application Layer
ECC	Experimental-Co-Computer
F3S	Flexible Sensor Simulation Suite
FOV	Field of View
HMD	Helmet Mounted Display
HMI	Human Machine Interface
LIDAR	Light Detection And Ranging
SCC	Sensor-Co-Computer
SLAD	Safe Landing Area Determination

Symbols

c_i	constants
e	Oswald factor
g	Earth's gravity, m/s^2
l	Length, m
m	Mass, kg
n	Load factor
R	Radius, m
S	Surface, m^2
t	Time, s
v	Velocity, m/s
x, y, z	Cartesian coordinates, m
Φ, Θ, Ψ	Roll, Pitch, Yaw angles
ρ	Density, kg/m^3

Indices

H	Helicopter
R	Rotor
S	Straight-in
T	Turn
TAS	True airspeed

1. INTRODUCTION

Landing on unprepared sites is a typical mission task in day-to-day helicopter operations. Right after the event of an emergency which requires an immediate landing, the choice of a proper landing site is one of various time-critical and vital tasks which a helicopter pilot has to handle under intensive stress.

Modules for landing zone detection and landing site ranking have been developed by DLR within the project HELI-X*. DLRs contribution to this project covered information fusion, planning of landing trajectories, trajectory following control, landing site display in a helmet mounted display (HMD) and preliminary studies on autorotation (AR) assistance.

*HELIcopter Situational Awareness for eXtreme mission requirements, funded by the Federal Ministry of Economics and Technology (BMWi) of Germany in the National Aerospace Research Program (LuFo IV) from 2012 to 2014

1.1. Related Work

Selecting a suitable landing site for aerial vehicles has been studied intensively in the past decade. Rotorcraft research in this area has been mainly driven by the development of an Autonomous Aerial Cargo/Utility System by the Office of Navel Research in the US. The topics of Safe Landing Area Determination (SLAD) [1] - [3] and automatic (emergency) landings [4] are addressed. Most recent progress is presented in [5] describing the design of the Tactical Autonomous Aerial LOgistics System (TALOS). Additional related work in the field of simulating autorotation (AR) flight dynamics and trajectory generation has been presented for helicopters in [6] - [8], and for autogyros in [9].

Further ideas considering landing site selection have been presented for indoor aerial vehicles [10] and unmanned rotorcraft [11, 12]. A method of comparing SLAD algorithms is presented in [13].

Emergency landing system designs have been proposed for General Aviation as well. An emergency-related algorithm for light aircraft based on a modified Rapidly Exploring Random Tree (RRT) [14] algorithm and Dubin's curves was presented in [15]. A commercially available application named XAVION[†] using a tablet computer has been developed by Laminar Research as a low-cost retrofit solution for private pilots. Both rely on a known environment provided by digital elevation maps.

During spacecraft operations on extraterrestrial surfaces the choice of an appropriate landing site is an important mission element as well. Additional constraints like mean sunlight exposure have been a topic in the ROSETTA[‡] named spacecraft mission.

1.2. DLR Activities

Recent projects dealt with the implementation of a full-scale pilot assistance system into the ACT/FHS [16]. During that period, a comprehensive sensor suite was integrated in the helicopter and certified for flight operation. The installed sensor system consists of a forward looking LIDAR with a field of view (FOV) of 31.5° (lateral) x 32° (vertical) and a detection range between 50 m and 1 km (see Fig. 1), a radar, an infrared and a TV camera.

The system is controlled by a cluster of Sensor-Co-Computers (SCC), which are running the software *SCC-Control* for data acquisition, recording and display rendering. A detailed overview of the architecture of the sensor suite is given in [17]. Additionally, the *Flexible Sensor Simulation Suite* (F3S) was developed by the Institute of Flight Guidance, which is capable of simulating all of the sensors mentioned before in real-time [18] - [20].

Flight tests have been conducted in the period from 2011 to 2013 and in 2015 with the sensor suite installed. The resulting comprehensive database of more than 10 hours of LIDAR, camera and navigational data recordings is used for research and algorithm development.

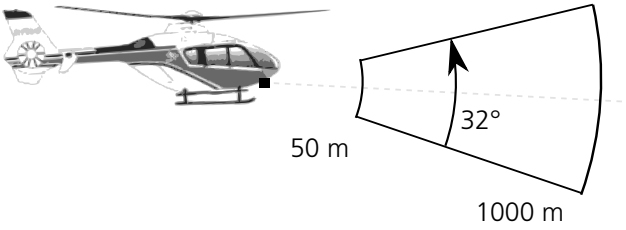


Figure 1: ACT/FHS with LIDARs FOV in side view.

In spring 2014 the Air VEhicle Simulator (AVES), DLR's new research flight simulator [21] was put into service. It is used for hardware, software, human-in-the-loop testing and for flight test preparation.

2. LANDING SITE DETECTION

Since the presented solution is part of the larger ACT/FHS's experimental system, the principal architecture is shown in Fig. 2. An additional overview of the involved modules and their task is given in Table 1.

Table 1: Software modules

Module	Task
SCC-Control	LIDAR data handling
Flatlander	Landing Site Identification
CoALa	Communication middleware
guARdian	Dynamic priorisation
F3S	Heightmap generation service

In order to detect an appropriate landing site the following steps are carried out:

A The module *Flatlander* initializes itself using a priori elevation and ground type data from available databases. Possible databases to be used can be SRTM [22], TANDEMX [23] or data in the GeoTIFF format. Examples of ground type data are shown later sections.

B During flight additional elevation data can be collected from sensors. These data are aggregated by *SCC-Control* and passed to *Flatlander* for fusion with the existing data.

C Triggered by an event (e.g. pilot request) the module *CoALa* defines a region of interest and the desired shape for *Flatlander*, which will look for appropriate solutions in the specified area. Additionally, a maximum

[†] www.xavion.com
[‡] http://www.nasa.gov/rosetta

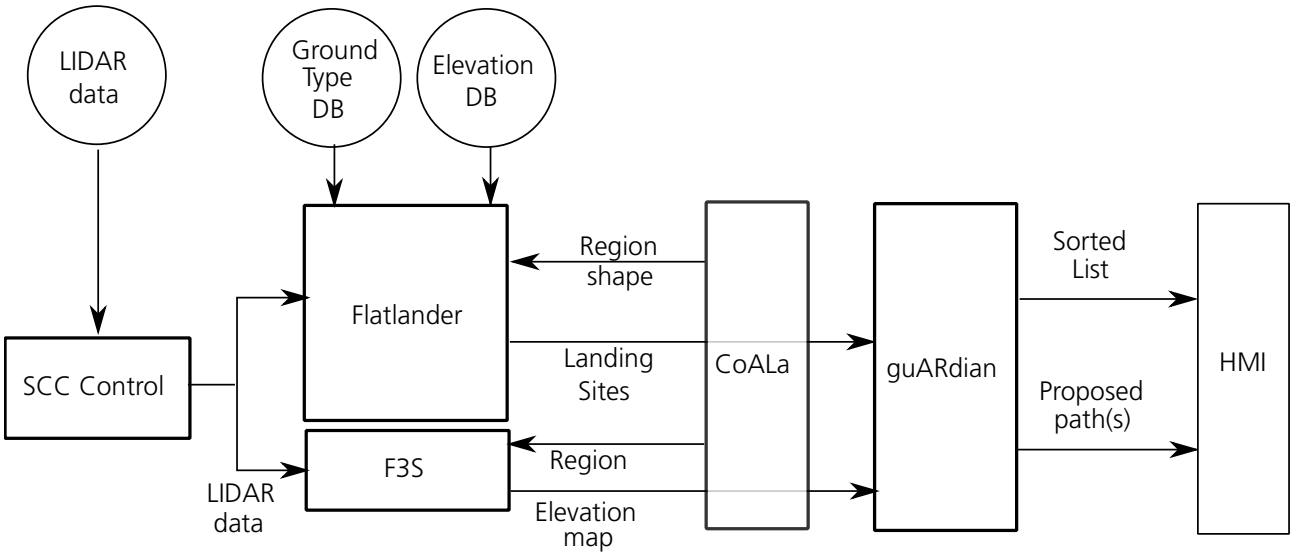


Figure 2: Modules involved in the experimental system of the ACT/FHS.

altitude can be defined to discard sites above the helicopter.

D Once *Flatlander* is initialized, *CoALa* asks once or periodically for a list of appropriate landing sites. For this, the maximal number of landing sites has to be specified.

E *Flatlander* delivers the list of possible landing sites within the region of interest that are in conformance with the shape and size specified earlier in the process.

F These solutions and a digital elevation map are handed over to guARdian for further decision making based on criteria described later in section 4.

G The resulting sorted list starting with the best landing site and one or multiple trajectory proposals can be handed over to a human machine interface (HMI), which is not part of this work.

2.1. Algorithm

The list of landing sites from *Flatlander* is generated using the following algorithm:

I Generate an elevation image of the region of interest. This is done by sampling the elevation database at the intended target resolution using metric, Euclidean coordinates as seen in Fig. 3 (a).

II Generate a template from the geometry parameters specified by *CoALa* (Fig. 3 (d)). This can be a circular disk shape or a filled rectangle with the specified orientation. Here, a preferred landing direction resulting from, e.g., the current wind direction can be taken into account by rotating the template in the proper direction. The resolution of the template has to match the resolution of the elevation image.

III Convert the elevation image into a gradient image containing local slopes (Fig. 3 (c)). This is done using image processing techniques from the OpenCV Framework[§], in our case a Scharr filtering [24].

IV Compute the convolution of the gradient with the template. The result is a template based matching (Fig. 3 (e)), that is, individual pixels of the result describe the average gradient length within the region of the template. A different interpretation is that each pixel contains a flatness measure: The lower the pixel value, the flatter the area within reach of the template.

V Let m be the maximum number of sites to deliver. Now the m smallest values in the matching image describe the locations of the best landing sites. Additionally, it is required that the resulting sites should not overlap and should contain only valid elevations. If we just used the m smallest value locations, these may be located closer together than the template size. Instead, an iterative approach is used. After calculating the smallest value location, the direct surroundings of this location are masked out in a mask image, so that these locations will not turn up in consecutive searches for the next smallest location. Furthermore, certain ground classes can be excluded, e.g. water bodies. This is done by looking up the ground class in the corresponding ground class map (Fig. 3 (g)). If any point in the template surroundings matches a forbidden class the location is discarded and masked out for later minimum searches. Figure 3 (f) shows the result without class restrictions. One can observe that some landing sites (e.g. the site marked with "1") overlap areas including roads, buildings, etc. Figure 3 (h) shows the result when restricting the search to agricultural areas only. Note that sites that were already located in agricultural

[§]www.opencv.org

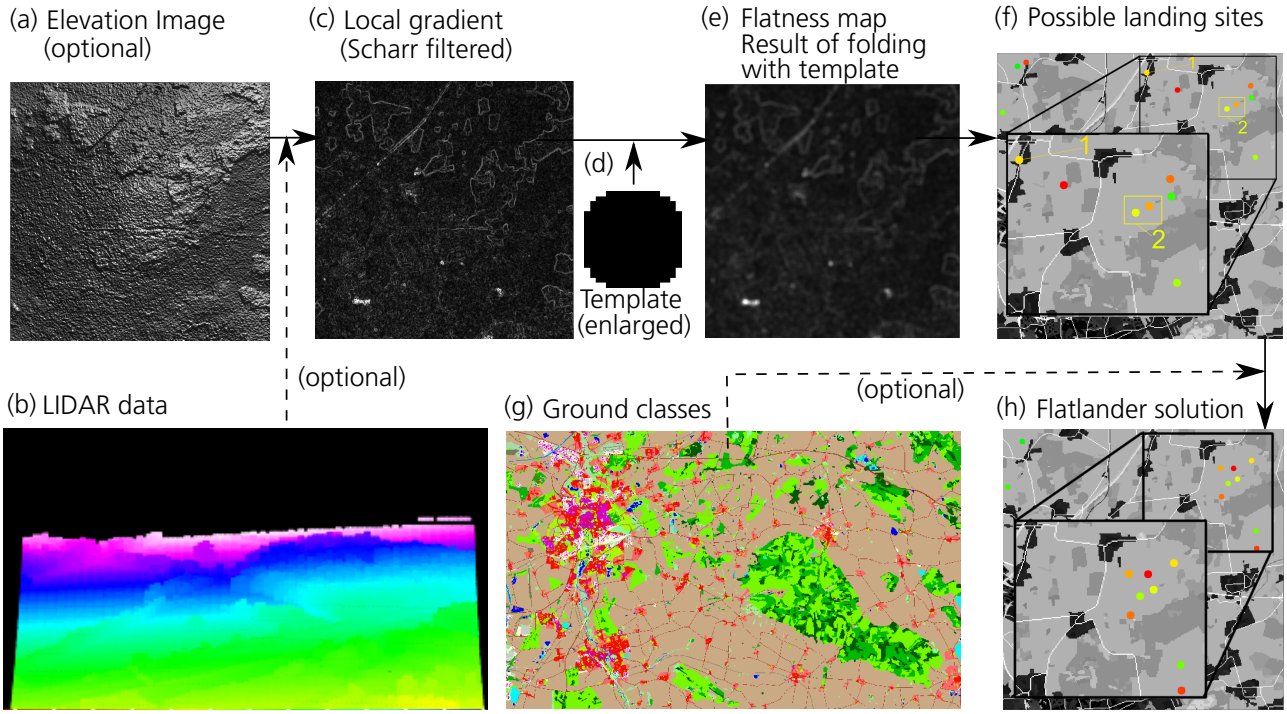


Figure 3: Intermediate results of *Flatlander* and different ground type data.

areas do not change their location (see "2" in Fig. 3 (f)) while others disappear and are replaced by different locations.

VI Compute a plane of best matching for each possible landing site in order to deliver the normal vector, slope and variance for the site.

2.2. Using LIDAR Data

The above description outlines the algorithm using elevation data taken from databases. Because these databases may be outdated, incomplete or both, the use of ACT/FHSs LIDAR data was implemented in *Flatlander*. This allows the module to restrict the search to areas which have already been sensed. Note that ground type class filtering based on a priori data is still applicable here. Results of LIDAR restricted search for circular templates without class restrictions are shown in later sections.

Possible solutions are marked with a numbered circle and coloring is gradually blended from green to red based on the goodness. This is defined as weighted sum of variance and slope ($goodness = 5 \cdot variance + slope$), which have been calculated in step VI in the last subsection. This search restriction to sensed areas only is a key component of the emergency ranking described later.

3. BASIC FILTERING

Now that the module for pre-selecting landing sites is described, it is applied to different test cases.

For first tests of the toolchain related to landing sites, a test scene (see Fig. 4) was built into AVES, taking into account suggestions from HELI-X project partners at Airbus Defense and Space. Its overall real-world dimensions are 250 m x 250 m and it is divided into 25 sub-sets of 50 m x 50 m. The parameters related to this landing site within this subset vary as follows: The slope increases in each column by 5° from 0° to 20°. Obstacle number and density is increased in each row by using equally spaced grids of cubes. Small cubes are of 10 cm and large ones of 50 cm edge length respectively. The first row contains no cubes, the second contains 25 small and the third 25 large cubes. The fourth column contains 25 small and 16 large cubes. All of the cubes in column one to four are placed with 10 m spacing. Apart from that, in the last column the overall number of obstacles is increased to 49 small and 36 large ones by decreasing the spacing to 6.66 m.

The coloring of the sub-sets in Fig. 4 (middle) shows whether this site should be declared as acceptable by the algorithm. A checkerboard pattern is applied to the area to give a better spatial impression when rendering unshaded. This landing site test scene is included as a sub-scene in a larger general purpose test area in the AVES simulator. This 3D model called *Sensor Test Area* has been implemented in the AVES visual system

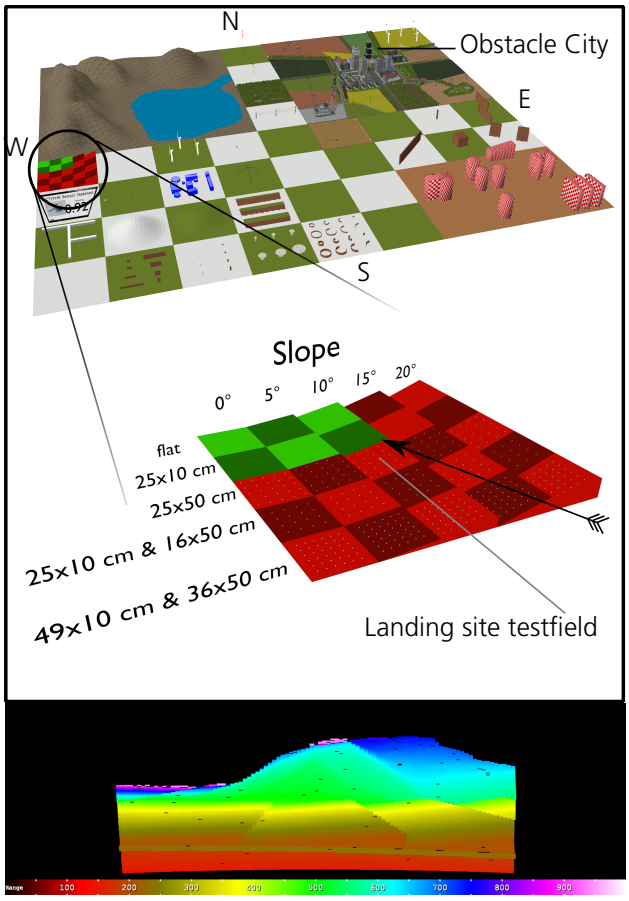


Figure 4: From top to bottom: DLR's sensor testarea, the landing site test field and a LIDAR data image during an approach from southern direction.

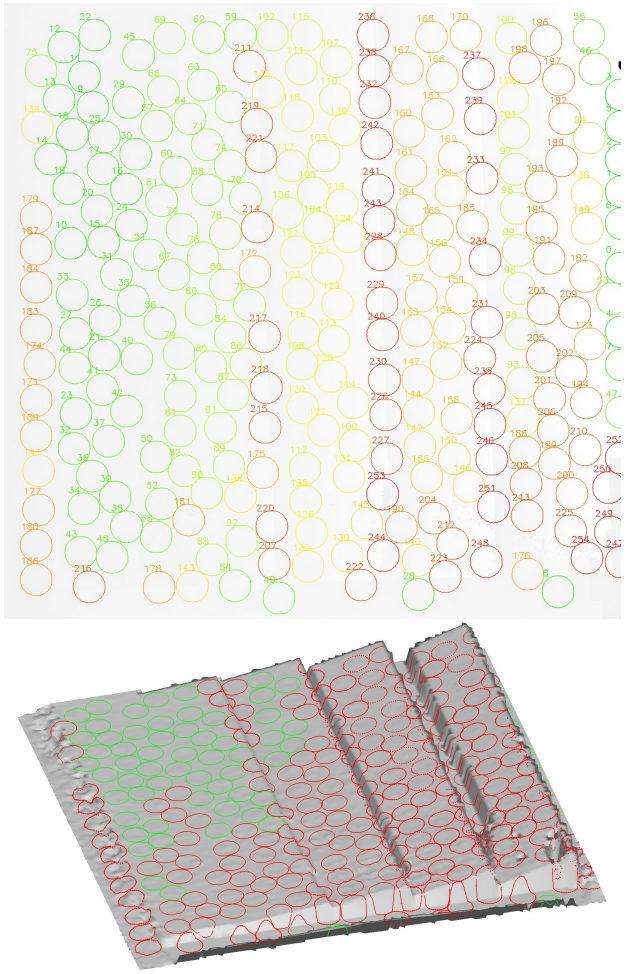


Figure 5: Top: *Flatlander* result for the landing site testfield. Bottom: Results drawn on a reconstructed height map of the area.

and in the sensor-simulation in mid 2014, shortly after AVES started operation. It includes a 1 km x 1 km urban scenario referred to as *Obstacle City*, which has been initially designed by an experienced pilot of the German Federal Police. Several isolated real-world scale obstacles and more generic test scenes are included as well. Its modular structure allows a quick modification for future use.

The setup used in this scenario is based on an approach from southern direction to the center of the landing site test field. During this approach LIDAR data of the scene in the FOV of the helicopter are simulated and passed on to the landing site toolchain (see Fig. 2). An image of the LIDAR data taken from *SCC-Control* can be seen in the bottom of Fig. 4. During the approach, the collected LIDAR frames are fed to *Flatlander* via shared memory for landing site identification and to *F3S* for custom-resolution height map generation.

The *Flatlander* result of the identified landing sites can be seen in Fig. 5 (top) with the $goodness$ based coloring described earlier. Due to the pre-defined spatial separation requirement there are several sites identified at the height discontinuities.

This result is handed over to guARdian with the height map, generated by *F3S* which can be seen in Fig. 5 (bottom). The MATLAB based report plots in Fig. 5 show a filtering based on maximal slope and variance. To reach a site acceptance close to the desired expectation as shown in Fig. 4, the maximum variance was set to $0.032\,m^2$ and the maximum slope was set to 11°. The sites that do not fulfill these limits are marked in red. An exceeding variance is visualized while drawing the site with a continuous line. In case the slope is exceeded, dot shaped markers are drawn. Note that there are sites in Fig. 5 which exceed both.

4. DYNAMIC EMERGENCY RANKING

First, a short summary of a pilot interview is given which outlines the basic motivation for the method chosen. Afterwards, the proposed algorithm and corresponding results are presented using a test case taken from DLR's

database.

4.1. Pilot Query

As key findings used for the development of *guARdian*, the following requirements for the ranking have been elaborated for landing site selection. As part of the project HELI-X, structured interviews with ten pilots have been conducted. The interviews are based on a literature review considering autorotation (AR). Key statements can be summarized in the following issues:

- Safety distances to the terrain except the near vicinity of the landing site have to be considered.
- Pilots prefer long final approaches.
- Pilots prefer approaches with headwind conditions.
- Pilots prefer paths with few curves in AR.
- Height loss during AR shall be considered.
- The decision making process needs to be fast.

The final approach is referred to as straight-in in the following. Based on these issues the design for the landing site ranking was developed.

4.2. Flight Test Data Case

As an example of the process a real-life testcase out of DLR's flight test database was selected. The prerequisites for this case have been:

- Complete coverage of terrain sensing.
- No false returns in LIDAR data.
- Critical obstacles on the scene.

The selected test case includes a sequence during a daytime enroute flight in western direction. While flying at an altitude of approx. 270 m above ground level, wind turbines and a forest appear in the sensor's field of view.

Data acquired by *SCC-Control* during the flight are shown in Fig. 6. The top view shows the image taken by the outside view TV camera. The two images below show a color coded LIDAR frame from the sensors' point of view (middle) and from a third person's perspective (bottom). In the bottom image the LIDAR points are color coded based on their difference to known elevation data. The wind turbines are clearly visible and marked with small letters for better comparison in later figures. Note that windturbine b is visible in the camera's FOV but not in the LIDAR's.

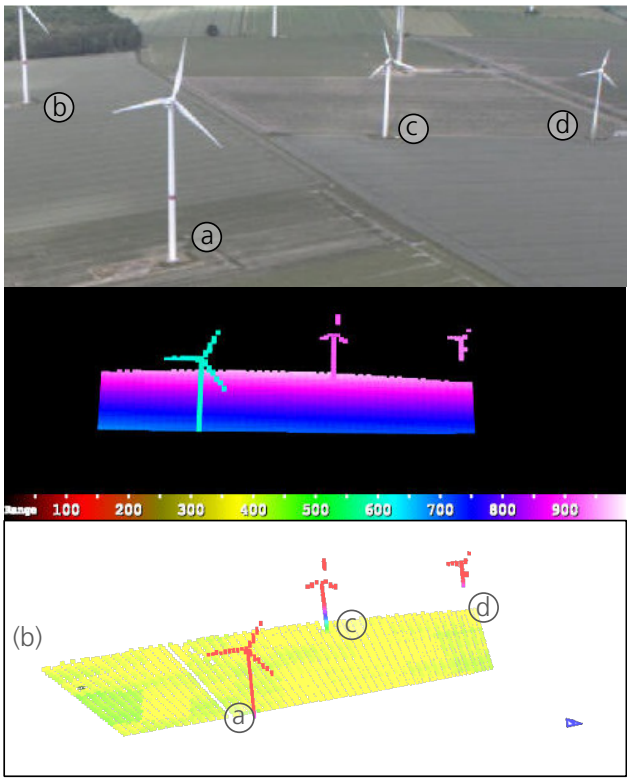


Figure 6: Flight Test case: Camera and LIDAR data at the windpark.

4.3. Algorithm

The system has to deliver a landing site proposal during a short time after an emergency. Therefore, it is designed as a preventive solution which is running passively during enroute flight. Because it is based on the acquisition of LIDAR data there has to be terrain within the sensor's range. This limits the operational use to low level flight only, depending on the sensors' range capabilities.

During LIDAR data acquisition, *Flatlander* (see Fig. 3) is asked periodically for possible landing sites in a rectangular area. The resulting sites identified by *Flatlander* in the region of interest at the windpark is shown Fig. 7. Afterwards, *guARdian* proposes a solution from these preselected sites while taking the above mentioned pilot preferences into account.

The algorithm used is divided into three main stages. Each of them is described in detail while referring to the figures showing intermediate calculation data. The stages are Initialization, per site analysis and ranking.

I Initialization

I.a A safety distance is added to the terrain. This is done by inflating the digital elevation map delivered by *F3S* by a pre-set range (here: 15 m). This gives a safe map (see Fig. 8) above the *F3S* map, which is used for collision checking later on.

I.b A set of initial turns for a number of load factors n (here: 1.01 to 1.7) is calculated. Turn start is set to be at the helicopter's position and propagate with discrete heading changes $\Delta\Psi$ either to the left or right of

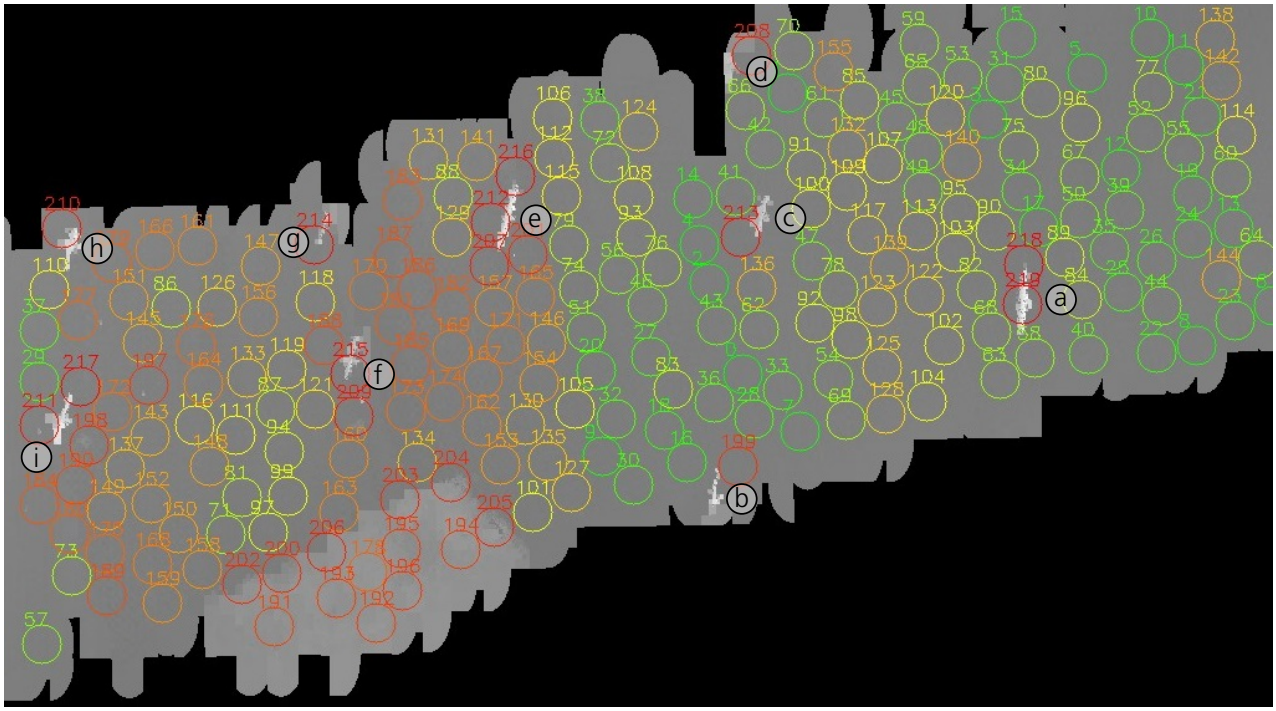


Figure 7: *Flatlander* solutions for a circular template with radius of 25 m in a 1600 m x 1000 m region of interest.

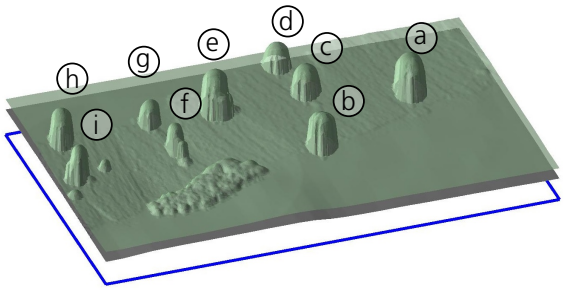


Figure 8: *F3S* map and inflated safe map.

the ground speed vector with the current true airspeed v_{TAS}. This is the first part of a chosen maneuver for a first response of the system, which is is a combination of a turn, followed by a straight-in approach. The height loss $\Delta z(v_{TAS}, n)$ is now described as a sum of the influence of the height loss during straight flight $\Delta z_S(v_{TAS})$ and the additional height loss during a turn $\Delta z_T(v_{TAS}, n)$.

$$\Delta z(v_{TAS}, n) = \Delta z_S(v_{TAS}) + \Delta z_T(v_{TAS}, n) \quad (1)$$

Using the load factor n, the resulting turn radius R_T can be obtained using flight mechanics ([25, chap. 7]):

$$R_T = \frac{v_{TAS}^2}{g\sqrt{n^2 - 1}}. \quad (2)$$

With Eq. (2) and the given trajectory discretization $\Delta\Psi$, the corresponding length of a segment (in the wind-fixed frame) is

$$\Delta l = R_T \Delta\Psi. \quad (3)$$

Using Eq. (3), the time it takes to travel along the discretization segment can be calculated as well.

$$\Delta t = \frac{\Delta l}{v_{TAS}} \quad (4)$$

Once these intermediate values for a given load factor and velocity are available, both factors for height loss can be obtained.

The height loss $\Delta z_S(v_{TAS})$ for straight flight is considered here by using a helicopter specific quadratic regression based on flight test data. In our case, based on data from 10 previously recorded flight tests of the ACT/FHS with speeds between 20 kts to 100 kts, an equation for the sink rate with respect to true airspeed was identified:

$$\dot{z}(v_{TAS}) = c_2 \cdot v_{TAS}^2 + c_1 \cdot v_{TAS} + c_0. \quad (5)$$

The constants identified for the sink rate (in ft/min) are summarized in Table 2, when v_{TAS} is given in kts. By

Table 2: Constants for sink rate regression

Constant	c_2	c_1	c_0
Unit	0.4241	-53.07	3676
Value	0.4241	-53.07	3676

using the results from Eqs. (4) and (5), Δz_s can finally be calculated with

$$\Delta z_S = \dot{z}(v_{TAS})\Delta t. \quad (6)$$

The second influence is the additional height loss during turns in AR due to the load factor. In [26], the following equation for the loss of height in AR is derived:

$$\Delta z_T(n) = \frac{m_H \Delta\Psi v_{TAS}^2}{2\rho S_R e g R_T}. \quad (7)$$

Combining Eqs. (2) and (7) and simplifying gives:

$$\Delta z_T(n) = \frac{m_H}{2\rho S_R e}\sqrt{n^2-1}\Delta\Psi \quad (8)$$

Neglecting a change in the helicopter mass m_H and air density ρ, the fraction in Eq. (8) can be seen as a constant.

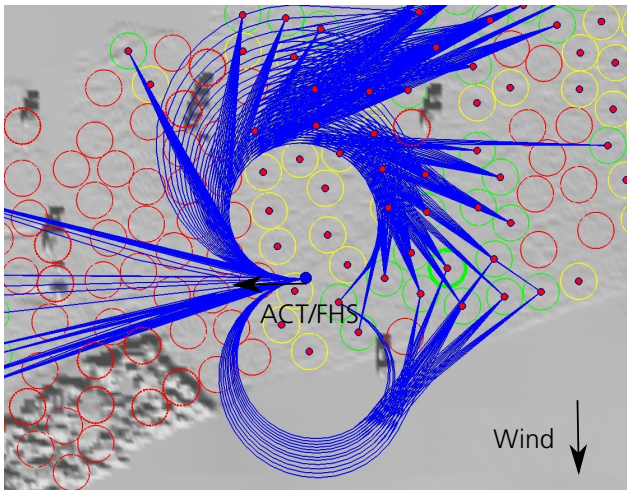


Figure 9: Flight test case - top view showing first response maneuvers. Red dots are observer points at sites with acceptable slope and variance.

Knowing the time t traveled at a discretization point and the wind vector, the circular paths can be transformed from the wind-fixed reference frame to the geodetic frame. This leads to trochoidal shaped trajectories and a corresponding direction vector for each point. The curved parts of the trajectories are shown in Fig. 9. In case the distance between two discretization points is larger than the grids spacing, additional points are sampled in between for collision checking. Once one point hits the safe surface, leaves the map or a heading change limit is reached (here: two full turns), it is proceeded with the next load factor.

This choice of a maneuver does not violate the preferences stated by the pilots during the earlier mentioned interviews. However, circle-line-circle connections like Dubin's curves or more sophisticated maneuvers can not be considered with this method.

II Per Site Analysis

Final straight connections to possible landing sites are assigned in the second stage for each site individually. Here, each of the sites delivered by *Flatlander* is analyzed. The currently analyzed site is referred to as the *active* site in the following.

II.a At first the delivered slope and roughness is compared to maximum allowed values. In case these values are exceeded, the active site is skipped. In Fig. 9 and 11, these are marked in red. In contrast to the synthetic environment, the limits in the flight test data case were set to a maximum variance of 0.8 m^2 and a slope of 8°.

II.b If the active site has passed above checks, its horizontal distance to the helicopter is calculated. In case it is larger than a preset value (here: 600 m), it is skipped and marked in gray (see Fig. 11). This is used to reduce the number of solutions when working with large maps.

II.c A copy of the safe map from the initialization is made and the safety distance is reduced locally around the active site.

II.d Based on the safe map and an observer point at a defined altitude above the site (see Fig. 9), the visibility hull for the landing point is calculated. This surface is an intermediate data structure proposed in [27]. The algorithm used traverses the map in a ring-wise manner, starting from the landing site. Since an interpolation pattern and no trigonometric function is used to propagate the surfaces' slope outwards, calculation times for a map of the dimensions shown are usually in the order of 10 ms. Once calculated, it divides the space above a map in two parts. Above this surface in 3D-space a direct connection to an observer point is guaranteed to be possible, below it is not. Figure 10 shows the visibility hull for a site based on the current map. This allows a simultaneous collision and visibility check from an arbitrary point in the space above the map to an observer point by using an efficient table look-up.

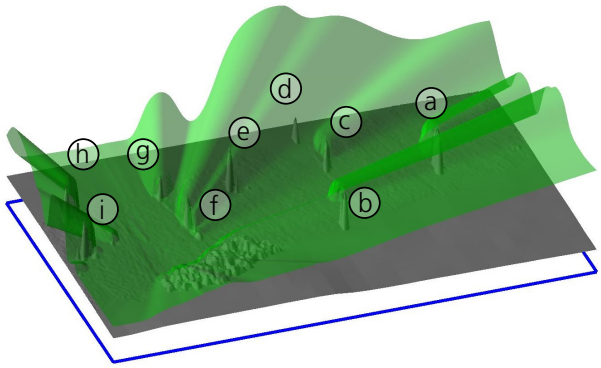


Figure 10: *F3S* map and visibility hull for a site between forest and windpark.

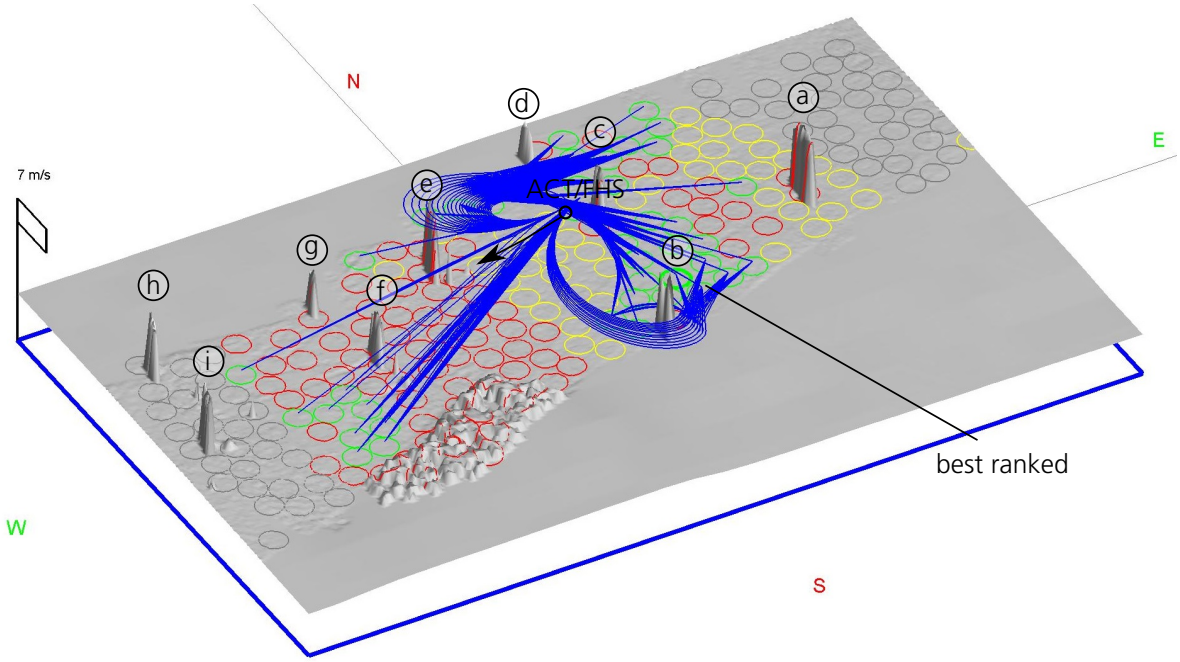


Figure 11: MATLAB report generated by guARdian under crosswind conditions.

II.e Now, once the temporary visibility hull is computed, the pre-calculated first response maneuvers are traveled point by point for each load factor. Once a point on a curve is found, which is above the visibility hull of the active site, it is further investigated. This is referred to as the active point.

A site is now checked for accessibility by using two criteria. First the expected heading direction at the active point shall be facing forward to the active site. In case it does, the track angle of the direct connection between the active point and the observer point is checked. Once this is between pre-defined limits (here: 15° to 35°), the site is marked as accessible (green) and the trajectory is drawn. There may be multiple solutions to reach a certain site as seen in Figs. 9 and 11.

In case there are straight-in solutions which lead to a landing with a deviation to wind direction of less than a threshold (here: 30°), this information is saved for later use in the ranking stage.

Landing sites which did not allow a trajectory solution in the previous step are marked as unaccessible and drawn (see Fig. 11, yellow circles).

III Ranking

Finally, once the information of accessibility and possibility of headwind landing is available for each site, the ranking stage starts, which is further divided in subtasks.

III.a The list of lateral distances between the sites is calculated. For each site a list of closest neighbors is saved.

III.b Finally a ranking (score) is given by the following scheme:

- 5 points for accessibility
- 10 points, in case a first response maneuver with headwind exists. This strong weighting is used to produce a pilot-like choice of landing into wind direction.
- 0.5 points for each accessible site within a certain distance (here: 100 m). When several sites are close to each other, this influence will prefer those with alternatives in the near vicinity.
- 3 points, in case the variance is very low (here: smaller than 0.3).

III.c This list of sites is sorted by score - the first one in the list is marked with a thicker green line in Fig. 11 and declared as the best ranked.

The testing took place on a standard Notebook PC with Intel i7 2.8 GHz CPU and 4 GB of RAM.

4.4. Wind Variation

Since pilots prefer landing with headwind during the approach, especially in AR, the above mentioned en-route test case is re-used to demonstrate the ranking developing over time and with varying wind conditions. The wind is set to be of the same magnitude (7 m/s) but from either crosswind or backwind direction. The results were obtained with the same scoring scheme and weights as described in the previous section.

In Fig. 12, a comparison of three timesteps along the

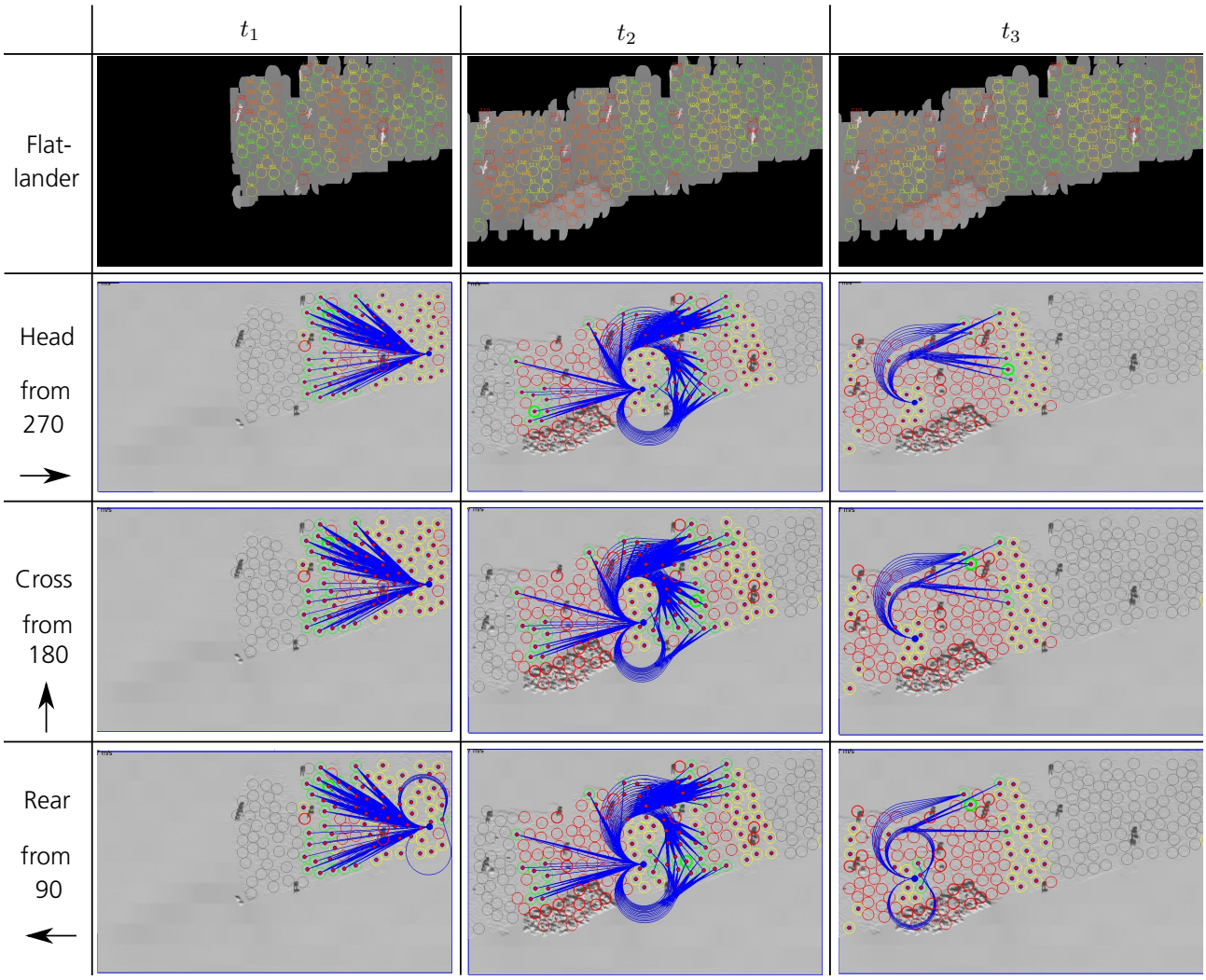


Figure 12: Overview of *Flatlander* and *guARdian* solutions with a wind of 7 m/s and changing direction.

flight is shown. The corresponding times are referred to as t_1, t_2 and t_3 respectively. At t_1 nearly half of the map was sensed and the helicopter is at the eastern border. It moves in western direction during t_2 and t_3 and *Flatlander* delivers more possible landing site solutions.

It can be observed that the expected accessibility of some sites may vary with changing wind conditions. Under rear-wind conditions, the site on the right border fulfills the criteria for accessibility due to the wind-shifting of the trajectory. The sites right below the helicopter under rear-wind conditions at t_3 are another example.

The map used here is not moving with the vehicle, which leads to the preference of some solutions, which do not have a straight-in with headwind conditions (see t_3 with wind from 270°). This drawback can be easily resolved by using moving grids in future development stages.

5. CONCLUSIONS

The results presented in the previous sections show that the system prototype is capable of prioritizing currently detected landing sites in a pilot-like manner. However, the environmental information gathered by the system described here relies on data acquired by a body-fixed LIDAR sensor. This may limit the usability due to two kinds of phenomena. These are either related to the body fixed mounting itself or involve false positive/negative LIDAR samples induced by environmental effects.

Since a human pilot can turn his head easily and guide his attention to varying areas of interest, the body fixed mounting allows only sensing in a narrow sector in the direction of the helicopter's longitudinal axis. For AR flight states this leads to several negative (NEG) and positive (POS) effects:

- **NEG:** The glide path angle during AR is steep (approx 15°), which may lead to loss of perception of

the currently flown flight path.

- **NEG:** During turns in AR the glide path angle becomes steeper, which amplifies the previous effect of looking above the path.
- **NEG:** The flight path is not in the FOV during more aggressive turns with small turn radii.
- **NEG:** During straight flight and crosswind conditions the stripe of sensed terrain is relatively narrow, which will lead to prioritization of sites at the borders of the sensed terrain.
- **POS:** Since the wind correction angle during enroute flight with crosswind yields to increased terrain coverage of the area which prefers headwind landings.

Concerning the type of sensor (LIDAR), two effects for landing site selection can be summarized:

- **NEG:** False positives may contaminate the point cloud database. These can be observed when the LIDAR is pointing to the sun during dusk or dawn daytimes or when fog or clouds are in the FOV.
- **POS:** No LIDAR returns are usually obtained from closed water surfaces like rivers or lakes. Because a landing on solid ground is expected to be preferred by pilots, this can be considered as a desired behavior.

These limitations could be circumvented by using a gimballed sensor with smart scanning pattern combined with LIDAR point filters.

6. OUTLOOK

Because the method so far represents a first prototype of a complex system, not all ideas during the development have been realized. The following list names a few possible future improvements.

- An AR dynamics model including more sophisticated energy considerations and flight dynamics (either online or pre-calculated maneuvers) may improve the solution.
- State prediction and transitions from enroute to steady AR and from steady AR to flare are not considered yet.
- An overlapping of sites should be acceptable to a certain percentage.
- No penalty is currently given for trajectories that lead through a-priori terrain, which may be possibly unsafe due to it's age or low resolution.
- Online ground classification like presented in [28] may further improve the choice of a solution.
- The vicinity to infrastructure (like streets) could be included as further rating criteria.

As some of the cited references state, there has already been research in this fields. By further developing these methods a contribution to increased situational awareness in low-level helicopter flight can be achieved.

7. ACKNOWLEDGMENT

As mentioned earlier, this work was mainly supported under the contract HELI-X. The contributions of colleagues at the DLR's Institutes of Flight Systems and Flight Guidance are greatly acknowledged. Related to the *Sensor Testarea* we would like to thank professional pilot Roger Dögow for the initial design of *Obstacle City* during the project SiRaSKoF-H[¶], and the AVES team for their continuous support during integration of the 3D model.

REFERENCES

AHS = American Helicopter Society International
AHSF = AHS Annual Forum and Technology Display

[1] Scherer, S., Chamberlain, L., and Singh, S., "Online Assessment of Landing Sites," *AIAA Infotech@Aerospace 2010*, Atlanta, GA, April 20-22, 2010. doi:10.2514/6.2010-3358.

[2] Chamberlain, L., Scherer, S., and Singh, S., "Self-Aware Helicopters: Full-Scale Automated Landing and Obstacle Avoidance in Unmapped Environments," *67th AHSF*, Virginia Beach, VA, May 3-5, 2011.

[3] Singh, S. and Scherer, S., "Pushing the Envelope - Fast and Safe Landing by Autonomous Rotorcraft at Unprepared Sites," *69th AHSF*, Phoenix, AZ, May 21-23, 2013.

[4] Choudhury, S., Scherer, S., and Singh, S., "Autonomous Emergency Landing of a Helicopter: Motion Planning with Hard Time-Constraints," *69th AHSF*, Phoenix, AZ, May 21-23, 2013.

[5] Paduano and others, "TALOS: An Unmanned Cargo Delivery System for Rotorcraft Landing on Unprepared Sites," *71st AHSF*, Virginia Beach, VA, May 5-7, 2015.

[6] Abbeel, P., Coates, A., Hunter, T., and Ng, A., "Autonomous Autorotation of an RC Helicopter," *Experimental Robotics*, Vol. 54 of *Springer Tracts in Advanced Robotics*, Springer, Berlin Heidelberg, 2009, pp. 385–394. doi:10.1007/978-3-642-00196-3_45.

[7] Yomchinda, T., Horn, J. F., and Langelaan, J. W., "Flight Path Planning for Descent-phase Helicopter Autorotation," *AIAA Guidance, Navigation, and Control Conference*, Portland, OR, Aug. 8-11, 2011. doi:10.2514/6.2011-6601.

[¶]funded by the civilian LuFo-IV research program of the German Federal Ministry for Economic Affairs and Energy

[8] Choudhury, S., Arora, S., and Scherer, S., "The Planner Ensemble and Trajectory Executive: A High Performance Motion Planning System with Guaranteed Safety," *70th AHSF*, Montréal, Québec, Canada, May 20-22, 2014.

[9] Galisteu, D. G., Adolf, F.-M., Dittrich, J. S., Sachs, F., and Duda, H., "Towards Autonomous Emergency Landing for an Optionally Piloted Autogyro," *71st AHSF*, Virginia, VA, May 5-7, 2015.

[10] Kushleyev, A., MacAllister, B., and Likhachev, M., "Planning for landing site selection in the aerial supply delivery," *2011 IEEE/RSJ International Conference on Intelligent Robots and Systems (IROS)*, San Francisco, CA, Sept. 25-30, 2011, pp. 1146–1153. doi:10.1109/IROS.2011.6094840.

[11] Holsten, J., Loechelt, S., and Alles, W., "Autonomous Autorotation Flights of Helicopter UAVs to Known Landing Sites," *66th AHSF*, Phoenix, AZ, May 11-13, 2010.

[12] Abershitz, A., Rubinets, R., and Gali, D. S., "Autonomous Landing of Unmanned Rotorcraft Aerial Vehicle - Laser Scanner Terrain Mapping," *AIAA Infotech@Aerospace Conference*, Seattle, WA, April 6-9, 2009. doi:10.2514/6.2009-1832.

[13] Takahashi, M. D., Abershitz, A., Rubinets, R., and Whalley, M., "Evaluation of Safe Landing Area Determination Algorithms for Autonomous Rotorcraft Using Site Benchmarking," *67th AHSF*, Virginia Beach, VA, May 3-5, 2011.

[14] LaValle, S. M., *Planning Algorithms*, Cambridge University Press, Cambridge, U.K., 2006.

[15] Fallast, A., "Automated Trajectory Generation and Airport Selection for an Emergency Landing Procedure of an CS23 Aircraft," *Deutscher Luft- und Raumfahrtkongress*, Augsburg, Germany, Sept. 16-18, 2014.

[16] Greiser, S., Lantzsch, R., Wolfram, J., Wartmann, J., Müllhäuser, M., Lüken, T., Döhler, H.-U., and Peinecke, N., "Results of the pilot assistance system "Assisted Low-Level Flight and Landing on Unprepared Landing Sites" obtained with the ACT/FHS research rotorcraft," *Aerospace Science and Technology*, Vol. 45, Sept., 2015, pp. 215–227. doi:10.1016/j.ast.2015.05.017, to be published.

[17] Lüken, T., Peinecke, N., Doehler, H.-U., and Lantzsch, R., "ALLFlight: tackling the brownout problem," *CEAS Aeronautical Journal*, Vol. 3, No. 1, Aug., 2011, pp. 1–15. doi:10.1007/s13272-011-0027-3.

[18] Peinecke, N., Döhler, H.-U., and Korn, B. R., "Real-Time Millimeter Wave Radar Simulation," *Journal of Aerospace Computing Information and Communication*, Vol. 10, No. 7, Juli, 2013, pp. 337–347. doi:10.2514/1.53403.

[19] Peinecke, N., Döhler, H.-U., and Korn, B. R., "Simulation of Imaging Radar Using Graphics Hardware Acceleration," *Proc. SPIE, Enhanced and Synthetic Vision*, Vol. 6957, Orlando, FL, March 17-20, 2008, pp. 695–720. doi:10.1117/12.782622.

[20] Peinecke, N., Lüken, T., and Korn, B. R., "Lidar simulation using graphics hardware acceleration," *IEEE/AIAA 27th Digital Avionics Systems Conference*, St. Paul, MN, Oct 26-30, 2008, pp. 4D41–4D48. doi:10.1109/DASC.2008.4702838.

[21] Duda, H., Gerlach, T., Advani, S., and Potter, M., "Design of the DLR AVES Research Flight Simulator," *AIAA Modelling and Simulation Technologies Conference (MST)*, Boston, MA, Aug. 19-22, 2013. doi:10.2514/6.2013-4737.

[22] Farr, T. G. et al., "The Shuttle Radar Topography Mission," *Reviews of Geophysics*, Vol. 45, No. 2, 2007. doi:10.1029/2005RG000183.

[23] Krieger, G., Moreira, A., Fiedler, H., Hajnsek, I., Werner, M., Younis, M., and Zink, M., "TanDEM-X: A Satellite Formation for High-Resolution SAR Interferometry," *IEEE Transactions on Geoscience and Remote Sensing*, Vol. 45, No. 11, 2007, pp. 3317–3341. doi:10.1109/TGRS.2007.900693.

[24] Scharr, H., *Optimale Operatoren in der digitalen Bildverarbeitung, PhD Thesis*, University of Heidelberg, Germany, 2000.

[25] Hull, D. G., *Fundamentals of Airplane Flight mechanics*, Springer Verlag, Berlin Heidelberg, 2007. doi:10.1007/978-3-540-46573-7.

[26] Holsten, J., "Simulation von Hubschrauber-Autorotationsflügen entlang generierter Trajektorien zu bekannten Notlandeplätzen," *Deutscher Luft- und Raumfahrtkongress*, Hamburg, Germany, Aug. 31 - Sept. 2, 2010.

[27] Srikanth, M. B., Mathias, P. C., Natarajan, V., Naidu, P., and Poston, T., "Visibility volumes for interactive path optimization," *The Visual Computer*, Vol. 24, No. 7-9, 2008, pp. 635–647. doi:10.1007/s00371-008-0244-x.

[28] Fitzgerald, D. and Walker, R., "Classification of Candidate Landing Sites for UAV Forced Landings," *AIAA Guidance, Navigation, and Control Conference and Exhibit*, San Francisco, CA, Aug. 15-18, 2005. doi:10.2514/6.2005-6405.